Journal of Alloys and Compounds 509 (2011) 9631–9637

Contents lists available at ScienceDirect

Journal of Alloys and Compounds

journal homepage: www.elsevier.com/locate/jallcom

Nucleation and growth kinetics of co-deposited copper and selenium precursors to form metastable copper selenides

John O. Thompson, Michael D. Anderson, Tim Ngai, Thomas Allen, David C. Johnson*

Materials Science Institute and Department of Chemistry, University of Oregon, Eugene, OR 97403, United States

ARTICLE INFO

Article history:
Received 25 October 2010
Received in revised form 14 July 2011
Accepted 15 July 2011
Available online 22 July 2011

Keywords:
Thin films
Chemical synthesis
X-ray diffraction
Calorimetry

ABSTRACT

The nucleation and growth kinetics of binary copper–selenium compounds from co-deposited copper and selenium films as a function of annealing temperature and time was investigated. The thermally driven evolution of crystalline phases was followed using differential scanning calorimetry and X-ray diffraction. Below 60% selenium, hexagonal α-CuSe formed during the deposition and a reversible endothermic transition at ~130 °C was observed for the phase transition into hexagonal γ-CuSe. Above 60% selenium the samples are amorphous as deposited and there is competition between the formation of γ-CuSe and cubic $CuSe_2$ as annealing temperature is increased. Slow rates of temperature increase favor the formation of $CuSe_2$ over γ-CuSe and near 66% selenium only cubic $CuSe_2$ forms during an exothermic event between 100 °C and 110 °C. It is surprising that the metastable cubic $CuSe_2$ initially nucleates and grows rather than the thermodynamically stable orthorhombic $CuSe_2$ polymorph. Kissinger analysis yields an activation energy for nucleation of 1.6 eV for cubic $CuSe_2$. CuSe nucleates throughout the composition region investigated. Hexagonal α-CuSe reacts with selenium to form the thermodynamically stable orthorhombic polymorph of $CuSe_2$ as the temperature approaches the melting point of selenium.

1. Introduction

In the electronics industry, circuits and display devices are built up by a sequence of deposited layers that often undergo various annealing steps during processing to arrive at the desired, often kinetically stable, structure. Since most films are deposited under conditions far from equilibrium, the structural changes and/or reactions of deposited films cannot be predicted solely from phase diagrams. Indeed, as early as 1958 Brewer [1] reiterated that it is very common for intermediate metastable phases to form before reaching a stable configuration, especially when the system is far from equilibrium. Qualitatively this can be considered as being caused by a local minimum on the free energy surface for the reaction, as indicated in Fig. 1. Providing energy into the system to overcome the smaller activation energy, $E_{a,1}$, for the metastable phase but not sufficient to overcome the larger activation energy, $E_{a,2}$, required to form the thermodynamic product traps the metastable product. In the 70s this concept was capitalized on by metallurgists seeking novel metallic glasses [2–4] and more recently metastable films precursors have been used to systematically prepare new compounds, understand nucleation barriers to compound formation and to better understand the energy landscapes made accessible by deposited films [5–17]. Understanding and controlling the evolution of deposited films is crucial for the successful manufacture of today's thin film electronic devices including solar cells, integrated circuits, and display technologies.

The manufacture of copper indium–gallium diselenide (CIGS) solar cells demonstrates the importance of controlling the kinetics during processing. CIGS based photovoltaic devices have been the subject of active research using a variety of synthetic approaches due to the desirable cost per watt brought about by the material's exceptional optical absorption coefficient and reasonable cell efficiency, as high as 18% [18–27]. To produce the most efficient CIGS solar cells, a three-step process is employed. A molybdenum coated glass substrate is heated and exposed to an indium–gallium–selenium flux that grows both on $(In,Ga)_2Se_3$ coating and creates a molybdenum diselenide layer as an ohmic contact. The flux is then shifted to copper and selenium, which converts the $(In,Ga)_2Se_3$ layer to a copper rich CIGS layer, the excess copper in the film having been shown to enhance grain growth in the film [21,28]. In the final step, additional indium is added to adjust film composition to avoid copper selenide impurity phases [18]. It is important to avoid copper selenide binary compounds in the final product as the presence of Cu–Se phases in the CIS provides recombination sites for the minority charge carriers, reducing overall cell performance [29–31].

The use of CuSe and $CuSe_2$ as precursors in the synthesis of and their presence as secondary phases in copper indium diselenide prompted this study of the nucleation and growth

* Corresponding author. Tel.: +1 541 346 4612; fax: +1 541 346 3422.
E-mail address: davej@uoregon.edu (D.C. Johnson).

0925-8388/$ – see front matter © 2011 Elsevier B.V. All rights reserved.
doi:10.1016/j.jallcom.2011.07.042

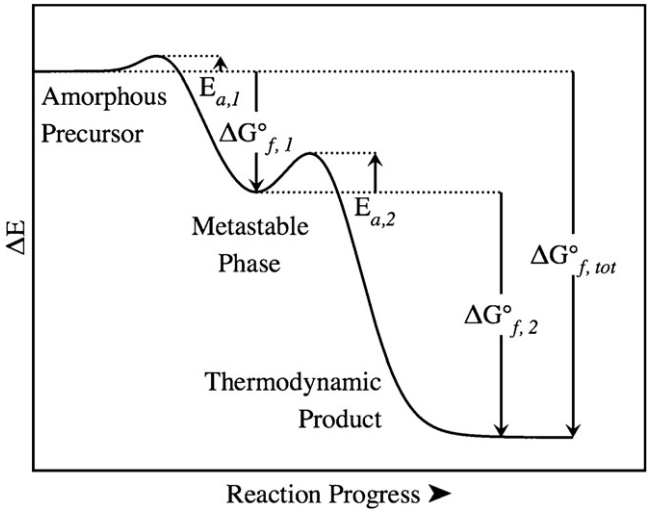

Fig. 1. Schematic diagram of the reaction path for formation of metastable intermediate phases from an amorphous precursor. There is a small activation energy, $E_{a,1}$, and small exothermic energy of formation, $\Delta G_{f,1}°$, for the metastable phase relative to the thermodynamic product. The actual stabilization or trapping of the metastable phase is enabled by a larger activation energy, $E_{a,2}$, to form the thermodynamic product.

kinetics of the selenium rich portion of the copper–selenium phase diagram. Copper selenium binary compounds have previously been investigated for their photovoltaic properties [29,32–36]. Additionally, CuSe has been used as a precursor layer for the formation of copper indium diselenide from a selenized stacked elemental layer [37–39]. CuSe and orthorhombic $CuSe_2$ have been identified as impurity phases in copper indium diselenide grown by electrodeposition and vacuum deposition processes [40–42]. Binary copper–selenium compounds have been made by several methods including melt techniques [43–45], mechanical alloying [46], electrodeposition [47], plasma-assisted selenization [48], and at aqueous–organic interfaces [49]. This paper examines the evolution of precursors prepared by co-depositing the elements on a cold substrate. Surprisingly, we observed the nucleation and growth of the metastable cubic phase of $CuSe_2$ over a broad composition range and are able to prepare single-phase samples of this metastable compound by controlling annealing conditions.

2. Experimental

The co-deposited copper selenium films described in this study were prepared in a custom built high vacuum chamber based on an earlier design [50]. Copper was deposited from an electron beam gun controlled by a quartz crystal thickness monitor. Selenium was deposited from an effusion cell with the flux monitored by a quartz crystal thickness monitor. The deposition rates of the two elemental sources were varied between 0.01 nm s^{-1} and 0.1 nm s^{-1} to achieve the desired compositions. The copper and selenium were simultaneously deposited onto a rotating 150 mm diameter silicon wafer located approximately 56 cm above the elemental sources. The wafer was coated with polymethylmethacrylate (PMMA), which was later dissolved in acetone to release the deposited material for collection on a filter paper and later use in DSC and XRD experiments. A small chip of silicon was also attached to the surface of the silicon wafer for use in compositional analysis. The target wafer was not actively heated or cooled during deposition. Film thicknesses for the as-deposited precursors were selected to ensure sufficient quantity of sample for analysis, on the order of 100–150 nm.

The composition of the co-deposited copper selenium samples was determined by electron probe microanalysis (EPMA) using the film deposited directly on silicon. A Cameca SX-50 microprobe was used to collect the X-ray emission data at three accelerating voltages from the thin film samples and standards consisting of elemental copper, selenium, and silicon. The X-ray emission counts from the copper–selenium thin films and the silicon substrate relative to the elemental standards were modeled using the Pouchou–Pichoir method [51,52] as implemented in the StrataGem software package [53] to determine the composition of the copper–selenium layer.

Heat flow from each copper selenium sample was quantified using differential scanning calorimetry (DSC). All DSC data was collected on a TA Instruments model 2920 DSC. Samples of the copper selenium films freed from the PMMA coated wafer were weighed and sealed in aluminum pans for analysis. Sample weights varied between 0.1 mg and 1 mg. Heat flow data was collected with the heated area under nitrogen to prevent sample oxidation. The DSC scans are shown with exotherms in the upward direction.

A Scintag XDS 2000 θ–θ diffractometer with a Cu Kα X-ray source was used to collect diffraction patterns and establish the presence and identification of crystalline phases in the as deposited and thermally annealed powder samples. Diffraction data from the flake-like samples demonstrated significant texturing, affecting the relative intensities of the diffraction maxima in the XRD patterns. Because of the significant texturing, Rietveld analysis of the phases in the samples was deemed impractical for the scope of this work and XRD patterns were compared to JCPDS patterns for identification purposes.

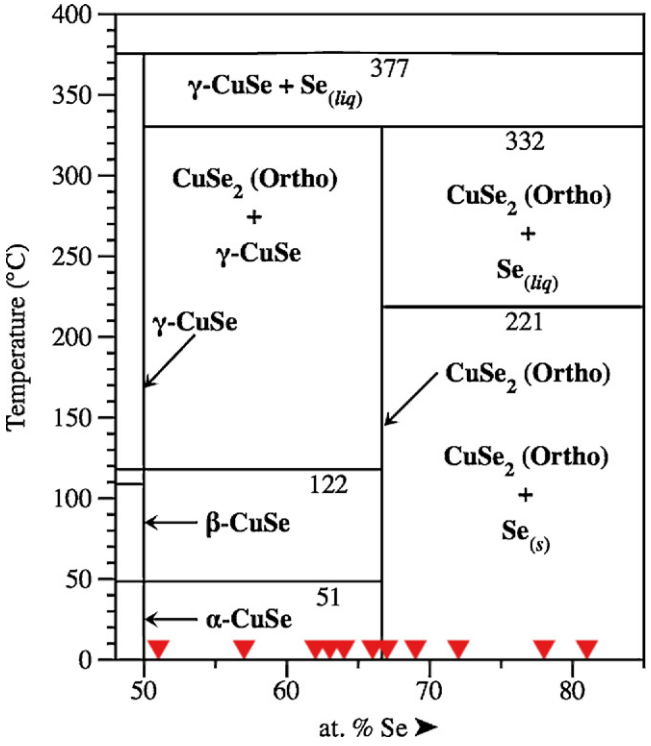

Fig. 2. Reproduction of the copper–selenium binary phase diagram [54] for compositions between 48% and 85% selenium. The red triangles located above the *x*-axis represent the compositions of samples prepared in this investigation as determined by EPMA analysis. (For interpretation of the references to color in the figure caption, the reader is referred to the web version of the article.)

3. Results and discussion

An initial suite of eleven samples were prepared by co-depositing the elements onto a cold substrate varying the ratio of the deposition rates to prepare samples between 51% and 81% selenium. The EPMA data for these samples demonstrated a uniform composition of the films across the substrate. The compositions of the samples are shown superimposed on the bottom axis of the phase diagram in Fig. 2. The phase diagram contains three copper–selenium compounds and the two more selenium rich compounds each have several polymorphs [43–45]. The most copper rich compound, Cu_3Se_2, was not observed in the composition range and annealing conditions we investigated. CuSe has three polymorphs. The form of CuSe stable at room temperature is hexagonal α-CuSe, which undergoes a reversible polymorphic change to orthorhombic β-CuSe at 51 °C. β-CuSe undergoes a reversible polymorphic change to hexagonal γ-CuSe at 120 °C. γ-CuSe peritectically disproportionates into β-$Cu_{2-x}Se$ and a selenium rich liquid phase at 377 °C. $CuSe_2$ has two polymorphs. The thermodynamically stable phase at atmospheric pressure is orthorhombic, is grown through slow cooling from a melt, and peritectically

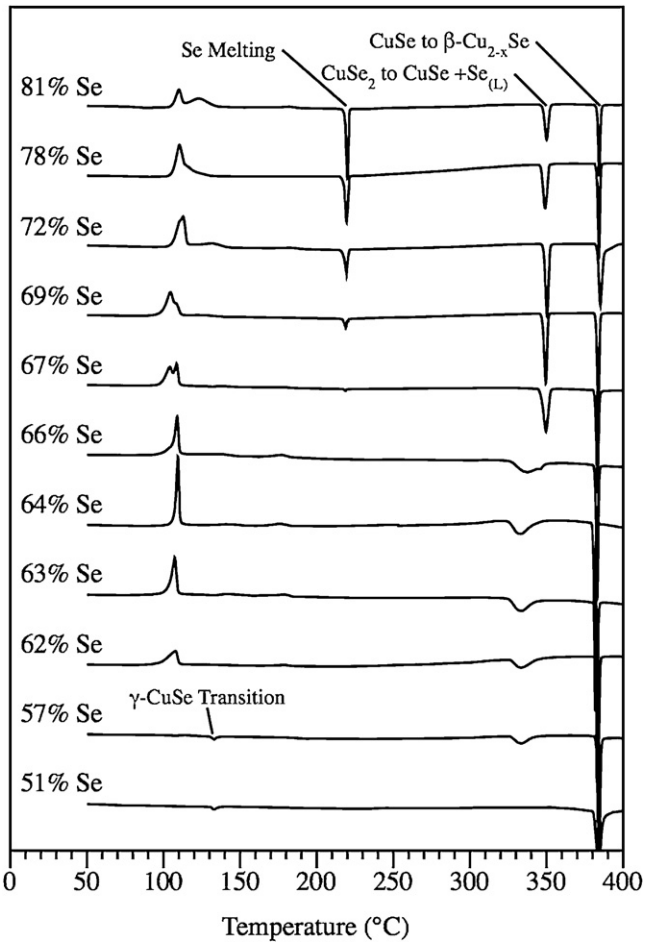

Fig. 3. DSC scans of co-deposited Cu–Se samples with compositions between 51% and 81% selenium performed at a heating rate of 4 °C min^{-1}. Exothermic transitions are indicated in the upward direction. Scans are arbitrarily offset vertically with percent of selenium, shown on the left, increasing as moved up the figure. The identities of the major endothermic transitions expected from the phase diagram in Fig. 1 are indicated.

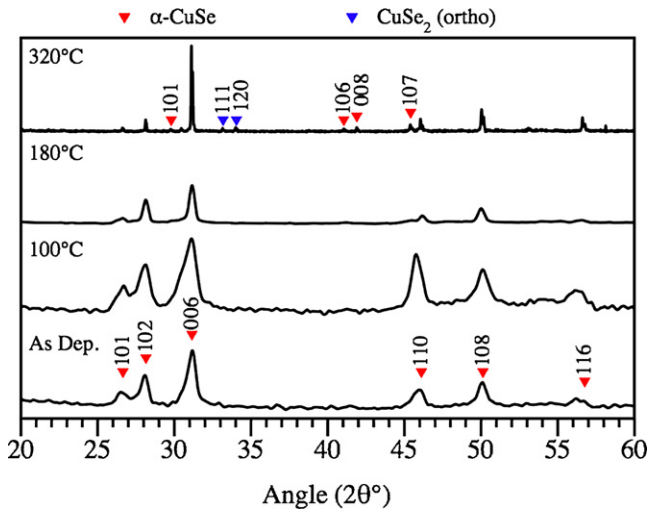

Fig. 4. XRD data for the sample containing 51% selenium annealed to indicated temperatures in a DSC at a rate of 4 °C min^{-1} and cooled. The numbers above the red triangles are the *h k l* indices of the diffraction peaks of hexagonal α-CuSe and the numbers above the blue triangles are the indices of the diffraction peaks for orthorhombic $CuSe_2$. (For interpretation of the references to color in the figure caption, the reader is referred to the web version of the article.)

disproportionates into γ-CuSe and a selenium rich melt at 332 °C [44]. The metastable polymorph is cubic and is prepared by annealing orthorhombic $CuSe_2$ at 12 kbar and 420 °C for 2 h followed by rapid cooling [44].

The phase diagram, however, does not predict the identity of compounds that will preferentially form from a co-deposited precursor with a specific composition nor does it predict the temperatures where compounds will form, which can be a function of prior annealing conditions and heating rate. Given the homogeneity of the film composition as determined by EPMA, crystallization events likely require an annealing induced fluctuation in the local composition. To probe the temperatures at which compounds form and the temperatures where phase transformations and decompositions occur, all of the samples prepared as part of this study were examined using DSC. Since the phase diagram is based on the formation of phases from a slowly cooled melt and the DSC scans in this study are on samples being slowly heated from a metastable precursor, the phase formation at low temperatures may not align with the phase diagram but equilibrium phases that have formed will undergo phase transitions at the temperature indicated on the phase diagram.

Fig. 3 contains the DSC scans of the initial eleven samples collected at a heating rate of 4 °C min^{-1}. As would be expected from the phase diagram, all of the scans contain an endothermic transition at 377 °C that corresponds to the decomposition of γ-CuSe to β-$Cu_{2-x}Se$ and a selenium rich melt. The behavior of the films below 377 °C enables us to roughly divide the samples into three different groups depending on the exotherms and endotherms observed in the DSC data. The five films containing 67% or more selenium all have endothermic transitions at 221 °C and 333 °C corresponding respectively to the melting of selenium and $CuSe_2$ decomposing into γ-CuSe and a selenium rich melt. The four films with compositions between 60% and 67% selenium all have a broad endothermic transition that starts below 333 °C and a slight exothermic transition at approximately 180 °C. The two films with compositions below 60% selenium have a small endothermic transition at approximately 130 °C, suggesting that α-CuSe has already formed in these films below this temperature. To identify the compounds forming at each of the exothermic and endothermic transitions observed in the DSC scans of all the samples, diffraction data were collected on samples that were annealed to indicated temperatures and then cooled to room temperature. The following paragraphs present and discuss the diffraction data collected on each group of samples and relate this data to the published Cu–Se phase diagram.

XRD data collected as a function of annealing temperature on a 51% selenium sample, which are representative of the data obtained on samples with compositions between 50% and 60% selenium, are shown in Fig. 4. The samples were annealed using a DSC scan to the indicated temperatures and cooled to room temperature for the diffraction scans. The two original and a second set of samples prepared with selenium composition between 50% and 60% were all found to have formed α-CuSe during the deposition process and all the diffraction peaks could be indexed to α-CuSe. In this compositional region, a small, reversible endothermic transition is present in the DSC scan at 130 °C, as indicated in Fig. 3. This endothermic transition may result from the β-CuSe to γ-CuSe phase transition which is expected at 120 °C, however, since we do not observe any heat signal for the α-CuSe to β-CuSe phase transition expected at 51 °C, it is possible that the 130 °C transition is for the conversion of α-CuSe to γ-CuSe. The narrowing of the diffraction peaks in Fig. 4, as a function of annealing temperature indicate grain growth of α-CuSe. After annealing at 320 °C, the size of the α-CuSe crystallites have significantly increased due to Ostwald ripening in the solid state and $CuSe_2$ appears as a minor phase as expected from the phase diagram. The amount of $CuSe_2$ increases in the diffraction

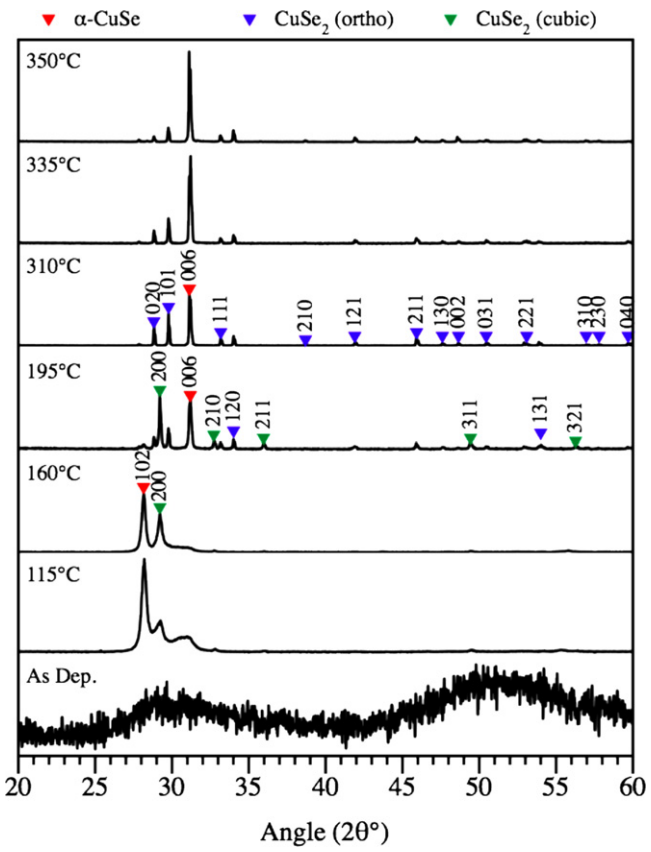

Fig. 5. XRD data for a sample containing 64% selenium and annealed in a DSC at a rate of 4 °C min^{-1} to the indicated temperatures and cooled to room temperature. The labels near the diffraction maxima are the indexed diffraction peaks of the observed phases.

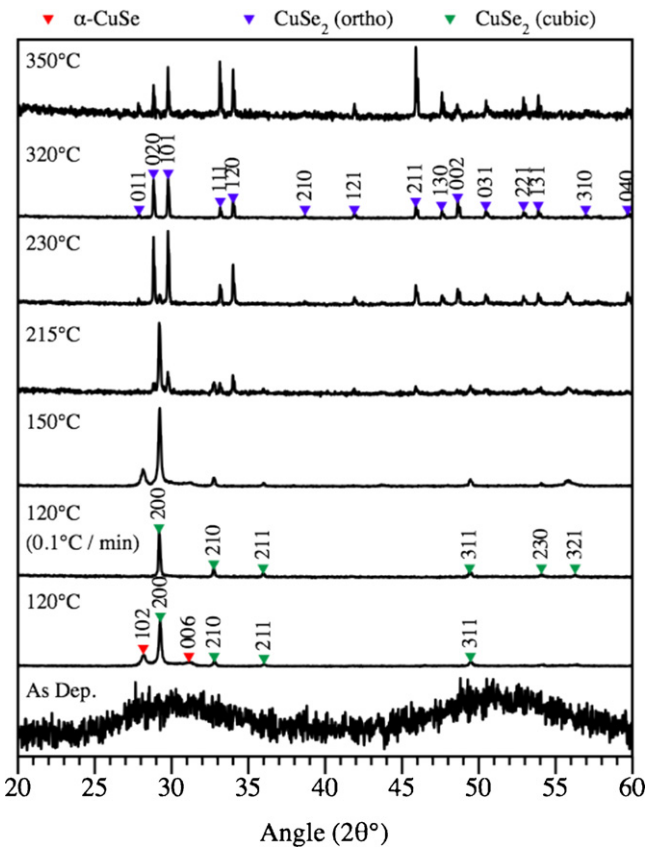

Fig. 6. XRD data for a sample containing 68% selenium and annealed to various temperatures in a DSC to the indicated temperatures and cooled to room temperature at the maximum rate experimentally accessible in the instrument. Scan rates are 4 °C min^{-1} unless otherwise indicated. The labels near the diffraction maxima are the indexed diffraction peaks of the observed phases.

patterns as the selenium concentration of the samples increases. A broad, reversible endothermic transition centered at 330 °C also appears in the DSC scans which increases in magnitude as selenium concentration increases up to 67% selenium. Murray [44] showed this transition to be the slow conversion of $CuSe_2$ to γ-CuSe and liquid selenium. Above 66% selenium, liquid selenium is present at these temperatures, and the broad endothermic transition is replaced by a sharp, reversible endothermic transition at 332 °C. This sharp endothermic transition is also from the reversible conversion of $CuSe_2$ to γ-CuSe plus liquid selenium as indicated in the phase diagram [54]. The temperature range and rate of this conversion is different for samples containing molten selenium versus those in a completely solid state and it is surprising that the solid-state reaction starts at a lower temperature.

The four films with compositions between 60% and 67% selenium all have an exothermic transition that begins below 100 °C and a slight exothermic transition at approximately 180 °C. Fig. 5 contains the XRD scans collected from a powder sample containing 64% selenium which are representative of the samples with selenium compositions between 62% and 66% selenium. The samples are X-ray amorphous as deposited and both CuSe and the metastable, high-pressure cubic polymorph of $CuSe_2$ have nucleated and grown after heating to 115 °C, past the irreversible exothermic event that begins below 100 °C. Since our diffraction data is collected after cooling the film back to room temperature, we do not know which polymorph of CuSe nucleates during this exothermic event, but it is surprising that the metastable, high-pressure cubic polymorph of $CuSe_2$ forms as well as CuSe. Diffraction scans collected on samples annealed above the 180 °C irreversible exothermic event show both grain growth of cubic $CuSe_2$ and the first appearance of the thermodynamically stable hexagonal $CuSe_2$ polymorph. At higher annealing temperatures we observe the broad, reversible endothermic transition centered at 330 °C discussed previously from the conversion of $CuSe_2$ to γ-CuSe and liquid selenium. Only orthorhombic $CuSe_2$ is apparent in the diffraction patterns after annealing to temperatures above this endotherm, with the relative intensity of the α-CuSe diffraction peaks varying as expected from the lever rule and the phase diagram. We do not observe the weak endotherm at 130 °C seen in samples with 50–60% selenium, presumably due to the small amounts of CuSe in these more selenium rich samples.

The DSC data of the five films containing 67% or more selenium differ from those containing between 60% and 67% selenium by having a broader exotherm with two heat flow maxima at around 100 °C, a reversible endothermic transition at 221 °C corresponding to the melting of selenium and a sharp endothermic transition at 333 °C. The slight irreversible exothermic transition at approximately 180 °C seen in the samples with 60–67% selenium is still observed, but only barely in some samples. Fig. 6 presents XRD data on powdered samples containing 68% selenium, representative for this group of samples, annealed in the DSC to temperatures near thermal transitions identified by the DSC scans and cooled to room temperature. These samples were observed to be X-ray amorphous on deposit. After the first irreversible exotherm near 110 °C, both α-CuSe and cubic $CuSe_2$ nucleate and grow. The presence of α-CuSe is surprising since it is not present at this composition in the equilibrium phase diagram and is observed to form even in samples with as much as 79% selenium. There is little change in the diffraction patterns until annealing past the irreversible 180 °C exotherm,

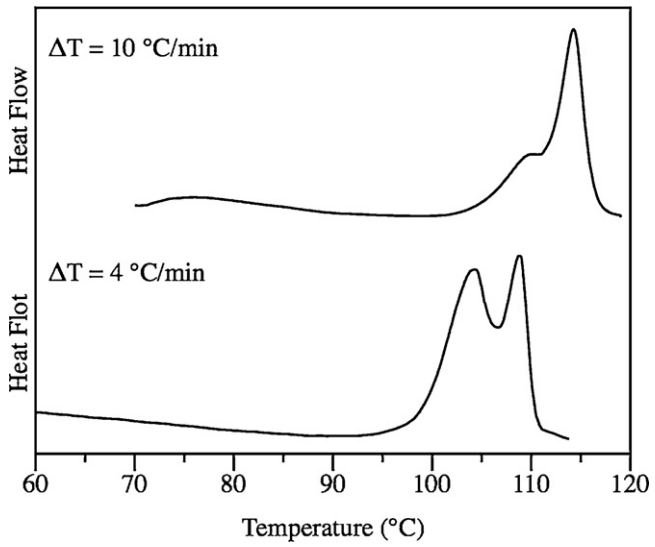

Fig. 7. DSC scans for 67% selenium samples at heating rates of 4 °C min^{-1} and 10 °C min^{-1}. The higher heating rate results in an increase in the magnitude of the second exothermic peak.

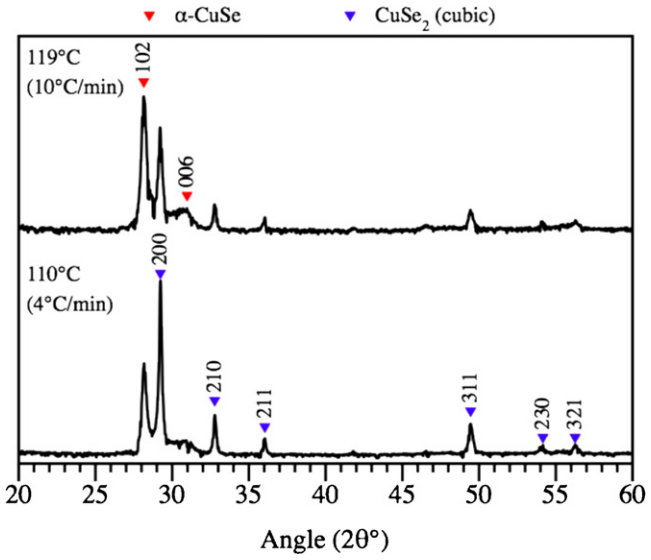

Fig. 8. XRD patterns of 67% selenium samples heated at 4 °C min^{-1} and 10 °C min^{-1}. The slower heating rate favors the formation of cubic $CuSe_2$.

after which the α-CuSe phase has disappeared and the orthorhombic polymorph of $CuSe_2$ is clearly present. The orthorhombic phase appears to form from the reaction of α-CuSe with the excess selenium and perhaps also from the conversion from the cubic phase of $CuSe_2$. The presence of selenium in these samples is indicated by an endotherm at 221 °C, the melting point of selenium, which becomes more pronounced with increased selenium concentration as expected from the phase diagram. The melting of selenium leads to grain growth of orthorhombic $CuSe_2$ and a large decrease in the relative amount of the cubic polymorph of $CuSe_2$ which can no longer be observed in the diffraction patterns after annealing to 320 °C.

The variation of the relative amounts of α-CuSe and cubic $CuSe_2$ observed after annealing through the 100 °C exotherm lead us to further investigate the competition between the nucleation of α-CuSe and cubic $CuSe_2$ with a sample containing 67% selenium. As seen in Fig. 3, the DSC at this composition has a distinctive double exotherm centered at 105 °C. Separate samples were heated at 4 °C min^{-1} and 10 °C min^{-1} to a temperature above the double exotherm with the DSC results presented in Fig. 7 and the XRD patterns that were collected on each sample presented in Fig. 8. The DSC results clearly indicate that a decrease in heating rate results in an increase in the magnitude of the first exotherm at the expense of the second. The XRD patterns indicate that the slower heating rate resulted in the formation of more of the metastable cubic $CuSe_2$ phase and less of the α-CuSe phase. This strongly suggests that the first DSC peak represents the nucleation of cubic $CuSe_2$ and the second is the nucleation of α-CuSe from the remaining amorphous part of the sample. Confirming this hypothesis, if the DSC heating rate is reduced to 0.1 °C min^{-1} almost phase pure cubic $CuSe_2$ is produced as shown in Fig. 6. The metastable cubic $CuSe_2$ phase nucleates at a lower temperature than the orthorhombic $CuSe_2$ phase.

The composition near 66% selenium is unique in that only cubic $CuSe_2$ forms during the first exothermic event between 100 °C and 110 °C as shown in the diffraction patterns contained in Fig. 9. Since only one phase forms during the 110 °C exothermic event, DSC data was collected at heating rates from 0.1 to 10 °C min^{-1} to determine the activation energy for nucleating cubic $CuSe_2$. Each sample was characterized by XRD to confirm that only the cubic $CuSe_2$ phase formed and to determine the a lattice parameter (0.6116(1) nm), which agreed with the published value [44]. Non-isothermal DSC data can be analyzed using a Kissinger analysis. In a Kissinger analysis, the activation energy is obtained from the peak temperature of the DSC exotherm, T_p, as a function of thermal scan rate Q [55]:

$$\frac{d\ln[Q/T_p^2]}{d\ln[1/T_p]} = \frac{-E_{cryst}}{R}$$

where R is the gas constant. Graphing $\ln[Q/T_p^2]$ versus $1000/T$ gives a straight line, as shown in Fig. 10, with a slope equaling $-E/R$ from which the activation energy for the nucleation and growth process is extracted. The activation energy for nucleation was determined to be 1.6 eV. The use of this equation requires, as has been indicated previously [56], a series of assumptions based on the nucleation mechanism, the composition of the amorphous and crystalline materials, and growth rate. Specifically, the equation presented above assumes that the growth process follows a Johnson–Mehl–Avrami relationship, has a uniform composition around the nucleation and growth event, and that that the nucleation and growth are constant for a given temperature.

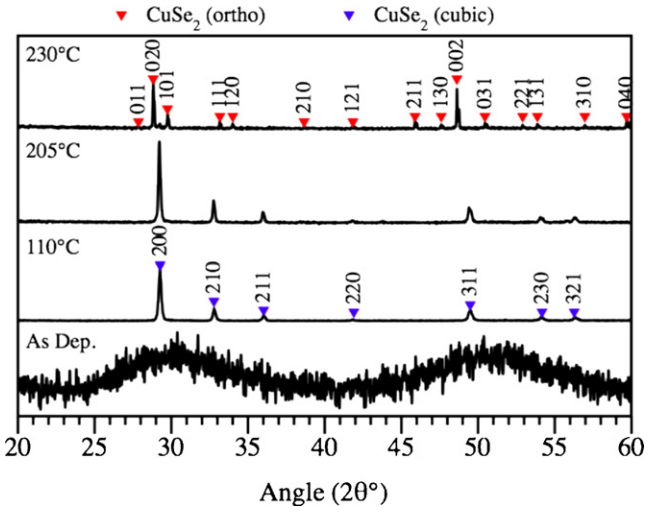

Fig. 9. XRD data for a sample containing 66% selenium annealed to indicated temperatures at a DSC at a rate of 4 °C min^{-1}. The labels near the diffraction maxima are the indexed diffraction peaks of the observed phases.

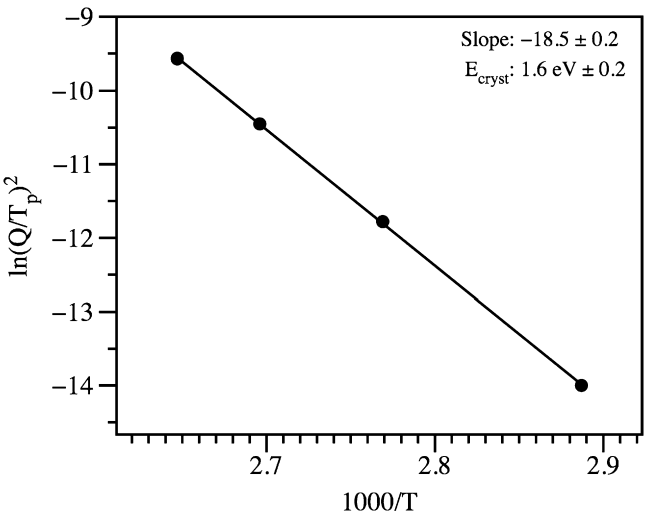

Fig. 10. Kissinger plot used to derive the activation energy for nucleation of cubic $CuSe_2$. DSC heating rates used for the Kissinger plot were 0.1, 1.0, 4.0, and 10 °C min^{-1}. The arguments of the logarithm were made unitless by dividing by the constant T_0^2/Q_0 where T_0 is 1000 K and Q_0 is 1 K min^{-1}.

The low temperature diffusion of copper in chalcogenides has been previously observed to lead to the crystallization and restructuring of copper selenium compounds over extended time periods under ambient conditions. Murray found that new XRD reflections appeared in a seven-year-old sample of CuSe, indicating a slow ordering process [44]. More recently, Ohtani produced Cu_3Se_2 in an ambient temperature solid-state reaction between α-CuSe and α-Cu_2Se over a span of several days [46]. The formation of the metastable cubic $CuSe_2$ at 100 °C and these prior reports prompted us to collect diffraction patterns on three powder samples that were stored in vials at ambient temperature for 44 months. The sample containing 72% selenium remained amorphous and the sample at 57% selenium remained unchanged with the presence of small CuSe crystallites. The sample containing 64% selenium crystallized both cubic $CuSe_2$ and α-CuSe with cubic $CuSe_2$ being the dominant phase. This further suggests that the metastable cubic $CuSe_2$ polymorph nucleates at low temperatures than the more thermodynamically stable orthorhombic form.

4. Conclusions

Examining the kinetics of phase formation of copper selenide compounds from co-deposited precursors lead to the discovery that non-equilibrium phases preferentially formed, demonstrating the importance of nucleation kinetics. α-CuSe was observed to form over a broad compositional range. This range extended beyond the region of the phase diagram where the α-CuSe phase is thermodynamically stable. α-CuSe is kinetically stable in films with compositions above 67% selenium at low temperatures, but decomposes on annealing above 140 °C by reacting with selenium to form orthorhombic $CuSe_2$. The low temperature nucleation of cubic $CuSe_2$, instead of the thermodynamically stable orthorhombic polymorph, was observed over a wide range of selenium rich compositions. The films with composition containing 66% selenium formed phase pure cubic $CuSe_2$ at heating rates up to 10 °C min^{-1}. At compositions close to this stoichiometry, the cubic $CuSe_2$ phase preferentially nucleated over α-CuSe at slow heating rates. Cubic $CuSe_2$ is also the first phase to form at compositions above 67% selenium and its growth forces the remaining amorphous material to become further selenium rich, making it more difficult to nucleate α-CuSe. The cubic phase showed lower thermal stability than previously reported, converting to the orthorhombic phase near 200 °C.

Acknowledgements

The research was funded by National Science Foundation under grants DMR 0907049 and CHE-0847970. MDA acknowledges support, in part, by the University of Oregon's National Science Foundation IGERT Fellowship Program under Grant No. DGE-0549503. JT acknowledges support of an NSF IGERT fellowship from grant DGE-0114419. This research was also funded in part by the Air Force Research Laboratory under agreement number FA8650-05-1-5041 and the Army Research Laboratory under agreement number W911NF-07-2-0083.

References

[1] L. Brewer, J. Chem. Educ. 28 (1958) 48–49.
[2] W. Johnson, S. Poon, P. Duwez, Phys. Rev. B 1 (1975) 150–154.
[3] W. Johnson, A. Williams, Phys. Rev. B 20 (1979) 1640–1655.
[4] A. Mogilatenko, F. Allenstein, M. Schubert, M. Falke, G. Beddies, W. Neumann, Mater. Sci. Forum 638 (2010) 2938–2943.
[5] T. Novet, D.C. Johnson, J. Am. Chem. Soc. 113 (1991) 3398–3403.
[6] L. Fister, D.C. Johnson, J. Am. Chem. Soc. 114 (1992) 4639–4644.
[7] J. Jensen, X. Kyablue, S. Ly, J. Appl. Phys. 94 (2003) 1252.
[8] J.M. Jensen, S. Ly, D.C. Johnson, Chem. Mater. 15 (2003) 4200–4204.
[9] C. Heideman, R. Rostek, M. Anderson, A. Herzing, I. Anderson, D. Johnson, J. Electron. Mater. (2010) 1–6.
[10] Q. Lin, M. Smeller, C.L. Heideman, P. Zschack, M. Koyano, M.D. Anderson, R. Kykyneshi, D.A. Keszler, I.M. Anderson, D.C. Johnson, Chem. Mater. 22 (2010) 1002–1009.
[11] N. Nguyen, P. Berseth, Q. Lin, C. Chiritescu, D.G. Cahill, A. Mavrokefalos, L. Shi, P. Zschack, M.D. Anderson, I.M. Anderson, D.C. Johnson, Chem. Mater. 22 (2010) 2750–2756.
[12] D. Fischer, M. Jansen, Angew. Chem. Int. Ed. 41 (2002) 1755–1756.
[13] T. Waniuk, J. Schroers, W.L. Johnson, Phys. Rev. B 67 (2003) 184203.
[14] M. Jansen, Angew. Chem. Int. Ed. 41 (2002) 3746–3766.
[15] Y. Liebold-Ribeiro, D. Fischer, M. Jansen, Angew. Chem. 120 (2008) 4500–4503.
[16] A. Risbud, L. Snedeker, M. Elcombe, A. Cheetham, R. Seshadri, Chem. Mater. 17 (2005) 834–838.
[17] M. Wuttig, N. Yamada, Nat. Mater. 6 (2007) 824–832.
[18] A.M. Gabor, J.R. Tuttle, D.S. Albin, M.A. Contreras, R. Noufi, A.M. Hermann, Appl. Phys. 65 (1994) 198–200.
[19] S. Gosavi, N. Deshpande, Y. Gudage, R. Sharma, J. Alloys Compd. 448 (2008) 344–348.
[20] Y. Kim, J. Lee, D. Shin, H. Chen, Photovoltaics Specialists Conference, 2009, pp. 001232–001233.
[21] M. Kim, R. Chalapathy, K. Yoon, B. Ahn, J. Electrochem. Soc. 157 (2010) B154.
[22] J. Xu, C. Lee, Y. Tang, X. Chen, Z. Chen, W. Zhang, S. Lee, W. Zhang, Z. Yang, ACS Nano 4 (2010) 1845–1850.
[23] P.P. Hankare, K.C. Rathod, P.A. Chate, A.V. Jadhav, I.S. Mulla, J. Alloys Compd. 500 (2010) 78–81.
[24] C. Wu, F. Chen, S. Lin, C. Lu, J. Alloys Compd. 509 (2011) 5783–5788.
[25] P.P. Hankare, A.S. Khomane, P.A. Chate, K.C. Rathod, K.M. Garadkar, J. Alloys Compd. 469 (2009) 478–482.
[26] M. Berruet, W.H. Schreiner, S. Ceré, M. Vázquez, J. Alloys Compd. 509 (2011) 3019–3024.
[27] A.R. Jeong, W. Jo, C. Ko, M. Han, S.J. Kang, M. Kim, D.Y. Park, H. Cheong, H.J. Yun, J. Alloys Compd. 509 (2011) 8073–8076.
[28] M. Contreras, B. Egaas, K. Ramanathan, J. Hiltner, A. Swartzlander, F. Hasoon, R. Noufi, Prog. Photovolt. 7 (1999) 311–316.
[29] C. Heske, R. Fink, E. Umbach, W. Riedl, F. Karg, Appl. Phys. Lett. 68 (1996) 3431–3433.
[30] S. Nishiwaki, N. Kohara, T. Negami, T. Wada, Jpn. J. Appl. Phys. 2 (37) (1998) 71–73.
[31] S.H. Wei, S.B. Zhang, A. Zunger, J. Appl. Phys. 85 (1999) 7214–7218.
[32] S. Lakshmikumar, A. Rastogi, Sol. Energy Mater. Sol. C 32 (1994) 7–19.
[33] M. Kharchenko, B. Boyko, P. Panchekha, A. Chernikov, V. Novikov, World Conference on Photovoltaic Solar Energy Conversion, vol. 1, 1998, pp. 504–506.
[34] H. Okimura, Thin Solid Films 71 (1980) 53–59.
[35] M. Schimmel, O. Bottechia, H. Wendt, J. Appl. Electrochem. 28 (1998) 299–304.
[36] G.B. Sakr, I.S. Yahia, M. Fadel, S.S. Fouad, N. Romčević, J. Alloys Compd. 507 (2010) 557–562.
[37] F. Hergert, R. Hock, A. Weber, M. Purwins, J. Palm, V. Probst, J. Phys. Chem. Solids 66 (2005) 1903–1907.
[38] F. Hergert, S. Jost, R. Hock, M. Purwins, J. Solid State Chem. 179 (2006) 2394–2415.
[39] S. Kim, W.K. Kim, R.M. Kaczynski, R.D. Acher, S. Yoon, T.J. Anderson, O.D. Crisalle, E.A. Payzant, S.S. Li, J. Vac. Sci. Technol. A 23 (2005) 310.
[40] M. Fahoume, H. Boudraine, M. Aggour, F. Chraibi, A. Ennaoui, J.L. Delplancke, J. De Physique Iv 123 (2005) 75–80.

[41] W. Kim, E. Payzant, S. Yoon, T. Anderson, J. Cryst. Growth 294 (2006) 231–235.
[42] T. Pisarkiewicz, H. Jankowski, E. Schabowska, Opto-Electron Rev. 11 (2003) 297–304.
[43] R. Heyding, Can. J. Chem. 14 (1966) 1233–1236.
[44] R. Murray, R. Heyding, Can. J. Chem. 53 (1975) 878–887.
[45] R. Murray, R. Heyding, Can. J. Chem. 110 (1976) 59.
[46] T. Ohtani, M. Motoki, K. Koh, K. Ohshima, Mater. Res. Bull. 30 (1995) 1495–1504.
[47] V. Garcia, P. Nair, M. Nair, J. Cryst. Growth 203 (1999) 113–124.
[48] S.T. Lakshmikumar, A.C. Rastogi, J. Appl. Phys. 76 (1994) 3068.
[49] C.N.R. Rao, G.U. Kulkarni, V.V. Agrawal, U.K. Gautam, M. Ghosh, U. Tumkurkar, J. Colloid Interface Sci. 289 (2005) 305–318.
[50] L. Fister, X.M. Li, J. McConnell, T. Novet, D.C. Johnson, J. Vac. Sci. Technol. A 11 (1993) 3014–3019.
[51] J.L. Pouchou, F. Pichoir, Scanning 12 (1990) 212.
[52] J.L. Pouchou, F. Pichoir, D. Boivin, Microbeam Analysis, San Francisco Press, San Francisco, 1990, p. 120.
[53] J.J. Donovan, T.N. Tingle, J. Microsc. 2 (1996) 1.
[54] T. Massalski (Ed.), Binary Alloy Phase Diagrams, vol. 2, ASM International, 1990, pp. 1475–1476.
[55] H.E. Kissinger, Anal. Chem. 29 (1957) 1702–1706.
[56] C. Johnson, K. Anderson, A. Gromko, D. Johnson, J. Am. Chem. Soc. 120 (1998) 5226–5232.